Amino acid-driven adsorption of emerging contaminants in water by modified graphene oxide nanosheets

N.B. When citing this work, cite the original published paper.

(article starts on next page)

PAPER

Check for updates

Amino acid-driven adsorption of emerging contaminants in water by modified graphene oxide nanosheets†

Sebastiano Mantovani,‡[a] Tainah Dorina Marforio, [iD] ‡[b] Sara Khaliha,‡[a] Angela Pintus,[a] Alessandro Kovtun, [iD] [a] Francesca Tunioli,[a] Laura Favaretto,[a] Antonio Bianchi,[a] Maria Luisa Navacchia, [iD] [a] Vincenzo Palermo, [iD] *[ac] Matteo Calvaresi [iD] *[bd] and Manuela Melucci [iD] *[a]

Graphene oxide nanosheets have shown promising adsorption properties toward emerging organic contaminants in drinking water. Here, we report a family of graphene oxide nanosheets covalently modified with amino acids and the study on their adsorption properties toward a mixture of selected contaminants, including pharmaceuticals, additives, and dyes. Graphene oxides modified with L-glutamic acid and L-methionine (GO-Glu and GO-Met) were synthesized and purified with a scalable and fast synthetic and purification procedure, and their structure was studied by combined X-ray photoelectron spectroscopy and elemental analysis. An amino acid loading of about 5% and a slight reduction (from 27% down to 14–20% oxygen) were found and associated with the adsorption selectivity. They were compared to unmodified GO, reduced GO (rGO), GO-lysine, and to the reference sample GO-NaOH. Each type of modified GO possesses a higher adsorption capacity toward bisphenol A (BPA), benzophenone-4 (BP4), and carbamazepine (CBZ) than standard GO and rGO, and the adsorption occurred within the first hour of contact time. The maximum adsorption capacity (estimated from the adsorption isotherms) was strictly related to the amino acid loading. Accordingly, molecular dynamics simulations highlighted higher interaction energies for the modified GOs than unmodified GO, as a result of higher van der Waals and hydrophobic interactions between the contaminants and the amino acid side chains on the nanosheet surface.

Water impact

Amino acid modification of graphene can open the way to the selective and high-capacity adsorption of emerging contaminants, including bisphenol A, in drinking water. The vision, in compliance to the water safety plans requested by the recent drinking water directives, is to select a specific biomodification to capture a specific targeted contaminant, *i.e.* chemical design toward predefined and tunable adsorption properties.

Introduction

In the last few decades, contamination of water sources has become more frequent all over the world. A vast array of

[a] Consiglio Nazionale Delle Ricerche, Institute for Organic Synthesis and Photoreactivity (CNR-ISOF), Via Piero Gobetti 101, 40129, Bologna, BO, Italy. E-mail: manuela.melucci@isof.cnr.it
[b] Alma Mater Studiorum – University of Bologna, Department of Chemistry 'G. Ciamician', via Selmi 2, 40129 Bologna, Italy
[c] Chalmers University of Technology, Göteborg, Sweden
[d] Center for Chemical Catalysis – C3 Alma Mater Studiorum – Università di Bologna via Selmi 2, 40126 Bologna, Italy

† Electronic supplementary information (ESI) available: Purification set up, molecular structure of selected contaminants, X-ray photoelectron spectroscopy (XPS), elemental analysis, adsorption selectivity and kinetic experiments, and adsorption isotherms. See DOI: https://doi.org/10.1039/d2ew00871h
‡ These authors contributed equally to this work.

pollutants, such as pharmaceuticals, personal care products, plastics, and additives, among others,[1–5] are not satisfactorily removed from water sources by conventional water treatment technologies. In the worst cases, this includes even drinking water.[6,7] This issue calls for the urgent development of new technology for detection, early warning, and remediation of those contaminants with proved eco- and human toxicity (such as perfluoroalkyl substances or bisphenol A).[8–11] Adsorption is the most promising strategy to enable the capture of emerging contaminants.[12–14]

Among the new sorbents emerging in the literature for water applications, graphene oxide (GO) is particularly advantageous as a sorbent. It can be exploited as a standalone material[15–19] or as an additive of polymeric membranes, in order to develop adsorptive membranes (*i.e.* membranes with synergic adsorption and filtration capability).[20–24]

Graphene oxide (GO) nanosheets have shown outstanding adsorption performances in terms of kinetic and adsorption capacities toward PFAS, methylene blue, and ofloxacin. For example, a maximum adsorption capacity of 356 mg g^{-1} of ofloxacin[25] was found for GO, i.e. an adsorption capacity 3.5 times higher than that of granular activated carbon (GAC), the industrial sorbent benchmark.[17] The maximum adsorption capacity of methylene blue for GO was found to be two times higher than that reported for activated carbon.[17] High adsorption efficiency was also demonstrated for reduced GO (rGO) at a short contact time (30 min), with values exceeding 99% for carboxylate and sulphonate PFAS with fluoroalkyl chain length from CF4 to CF13.[18]

However, a full understanding of the relationships between the structure and sorption selectivity/efficiency is needed to maximize the impact of graphene in water treatment. This requires an extensive investigation on different types of graphene nanosheets and a wide library of contaminants. Indeed, the adsorption strongly depends on the interplay of the surface area, surface chemistry, and morphology of the sorbent, and on the chemical structure of the targeted contaminants, which can change dramatically, even within the same family of contaminants (i.e. drugs, dyes, personal care products).[16]

For instance, the role of the oxidation degree in GO has been recently demonstrated by the synthesis of highly defected GO (i.e. GO with a prominent number of holes and defects on the surface).[17,26–28] The number of carbonyl and carboxylic groups, mainly located at the defect edges, increased directly with the number of holes.[17]

The key role of surface chemistry in the adsorption properties is also proved by the studies of selectivity and efficiencies of functionalized graphene-based sorbents, in comparison with unmodified graphene.[16,29] Losic et al.[29] recently summarized the results on different graphenic materials and rationalized the adsorption performance in relation to the surface area, pore size, type of functional group, and C/O, C/N, and C/S atomic ratios of the graphenic sorbents. For example, sulphonated graphene nanosheets showed enhanced removal of methylene blue with respect to graphene, thanks to the enhanced electrostatic interaction promoted by SO$_3$H groups.[30] Amino-functionalized graphene oxide (AGO) aerogels showed enhanced electrostatic interactions toward negatively charged perfluorooctanoic acid (PFOA),[31] with respect to unmodified GO, and consequently high removal (>99%) of PFOA from water. GO-based silica coated magnetic nanoparticles functionalized with 2-phenylethylamine (PEA) proved to be a good sorbent for organophosphorus pesticides in water thanks to the various chemical groups on the nanocomposite surface allowing hydrogen bonding and π–π interactions with electronegative atoms (P, N, and S) of the pesticides.[32]

Here, we report on the synthesis and structure–sorption property relationship of amino acid-functionalized GO. Amino acids are convenient building blocks to tune the surface chemistry of GO nanosheets thanks to their availability, small size, and large chemical variety. They can be covalently grafted on GO by following different routes, including amination or C–N coupling[33–36] with the epoxide or carboxylic functional groups, which are abundantly available on the surface of GO nanosheets. Previous studies reported the successful use of amino acid-modified GOs (both covalently and not covalently bound) for the removal of metals,[37–39] organic dyes,[40,41] and antibiotics.[42]

In this line, our group recently reported a facile and scalable synthesis of lysine-modified GO (GO-Lys) by amination through microwave-assisted epoxide ring opening reaction, and its purification by an unprecedented microfiltration approach.[43] We showed that modification with lysine enhances the removal capacity of bisphenol A (BPA), benzophenone-4 (BP4), and carbamazepine (CBZ) from tap water.

Starting from this evidence and aiming at a rational understanding of the adsorption mechanisms, here we report the synthesis of L-glutamic acid- and L-methionine-modified GOs (GO-Glu and GO-Met), their structural characterization, and the investigation on the role of the amino acid in the adsorption properties. The three selected amino acids have side chains of similar length but strongly different chemical properties. Indeed they are characterized by different charges at neutral pH (Glu: negative, Met: neutral, Lys: positive) and by different pendant groups, i.e. carboxylic (Glu), thioether (Met) or amine (Lys), enabling different types of intermolecular interactions. The structure–adsorption property relationships in the amino acid modified graphenic materials were investigated by a combined theoretical and experimental approach, which includes adsorption kinetic and selectivity tests, molecular dynamics simulations, and adsorption isotherms.

Experimental

Materials

Graphene oxide (GO) and reduced graphene oxide 80% (rGO) were purchased from Layer One (S-126/36) and used without further purification. L-Methionine methyl ester, L-glutamic acid monosodium salt monohydrate, ofloxacin (OFLOX), diclofenac (DCF), benzophenone-4 (BP4), carbamazepine (CBZ), bisphenol A (BPA), benzophenone-3 (BP3), rhodamine B (RhB), and caffeine (CAF) were purchased from Sigma-Aldrich and used without any further purification. Sodium hydroxide was purchased from Carlo Erba. LC-MS grade acetonitrile was purchased from Sigma-Aldrich in the highest available purity and used without any further purification. Plasmart 100 microfiltration modules (Versatile™ PES hollow fibers, cut off 150 nm, filtering surface 0.1 m^2, pore size 100–200 nm) were provided by Medica S.p.A (Medolla, Italy).[44]

Synthesis of GO-amino acid and purification

A basic solution of amino acid (L-glutamic acid or L-methionine methyl ester) was prepared by adding 930 mg of amino acid and 381 mg of NaOH to ultrapure water (13 mL).

The solution was then added to 62 mL of GO suspension (5 mg mL^{-1} in ultrapure water, sonicated for 2 h). The mixture was irradiated with microwaves for 3 h (T_{max} = 80 °C; P_{max} = 120 W), and then 5 mL of EtOH was added. The crude was purified by microfiltration on commercial Versatile™ PES modules, (Plasmart 100 module, Medica s.p.a.) according to previously reported conditions,[45] which are summarised in the sketch of Fig. S1, ESI.† A total volume of about 2 L of water was required to purify the crude obtained by using 0.5 g of GO as a starting material. The control material, GO-NaOH, was prepared by performing the same reaction but without the addition of the amino acids. 263 mg of GO-Met and 260 mg of GO-Glu were obtained after purification.

X-ray photoelectron spectroscopy (XPS)

High-resolution XPS was performed with a Phoibos 100 hemispherical energy analyser (Specs GmbH, Berlin, Germany), using Mg Kα radiation ($\hbar\omega$ = 1253.6 eV; X-ray power = 125 W) in constant analyser energy (CAE) mode, with an analyser pass energy of 10 eV. The base pressure in the analysis chamber during analysis was 4.2×10^{-8} mbar. The spectra were fitted by using CasaXPS (https://www.casaxps.com). Shirley background subtraction and all spectra were calibrated to the C 1s binding energy (285.0 eV). XPS samples were obtained by preparing a tablet from the dry powder of each material and fixing it on the sample holder with conductive carbon tape.

Elemental analysis (EA)

Elemental analysis was performed on modified GO powders by using an Elementar Unicube Elemental analyser, method GRAPHITE.

Scanning electron microscopy (SEM)

Scanning electron microscopy (SEM) analyses were performed with a ZEISS LEO 1530 FEG. The samples were deposited on a cleaned silicon wafer by dropping 100 μL of suspension at 0.1 mg mL^{-1} concentration in dimethylformamide. The energy of electrons was 5 keV and the signal was acquired using an inLens detector at a working distance of 3–5 mm.

Adsorption selectivity and kinetic experiments

A stock solution of eight emerging contaminants (CAF, OFLOX, BP4, CBZ, BPA, RhB, DCF, BP3) at 10 mg L^{-1} each was prepared in tap water. In a typical experiment, 25 mg of tested adsorbents (GO-Glu and GO-Met) were sonicated for 2 h in 5 mL of ultrapure water. After that time, 5 mL of the stock solution described above was added, to reach a final concentration of 5 mg L^{-1} for each contaminant. The solutions were gently stirred in the dark for 1 h, 4 h, and 24 h and then centrifuged at 15 000 rpm for 10 min. GO, GO-NaOH, and rGO were tested under the same conditions previously described.[43]

High performance liquid chromatography (HPLC-UV VIS)

Analyses of the treated water samples were performed by HPLC on a Dyonex Ultimate 3000 system equipped with a diode array detector. 0.5 mL samples were used as sources for the automated injection. The chromatographic separation was performed on a reverse phase analytical column (Agilent Eclipse XDB-C8 4.6 × 150 mm, 5 μm) at a flow rate of 1.0 mL min^{-1}, linear gradient TFA 0.05% aqueous solution/acetonitrile from 80 : 20 to 0 : 100, detection at λ_{max} of each analyte. In the case of the adsorption experiments on the selected emerging contaminants in the mixture, the percentage removal of the analytes was determined by comparison with that of the initial untreated solution. The results are expressed as the mean of two independent experiments ± SD.

Adsorption isotherm experiments

The adsorption isotherms of GO-Glu and GO-Met for BP4, BPA, and CBZ were obtained by varying both the concentration of contaminant and the amount of adsorbent. Stock solutions of each contaminant were prepared in ultrapure water, according to the maximum solubility of each molecule: BP4 1.0 mg mL^{-1}, BPA 0.3 mg mL^{-1}, and CBZ 0.1 mg mL^{-1}. For each sorbent, two suspensions were prepared, 2 mg mL^{-1} and 3 mg mL^{-1} in ultrapure water, and used after 2 h of sonication. A different amount of graphene suspension was added to a solution of contaminant (BP4, BPA, or CBZ) at different initial concentrations. The solutions (total volume 5 mL) were gently stirred in the dark for 4 h and then centrifuged at 15 000 rpm for 10 min. The solutions were analysed by UV-vis spectroscopy or HPLC (more details in the ESI†). The same procedure was performed for each pair of sorbent–sorbate, varying the ratio due to the different adsorption capacities. Each run was repeated twice on different batches of materials. Experimental parameters and details are reported in the ESI.† Isotherms of GO, GO-NaOH and GO-Lys were already reported.[43] Isotherms of rGO were obtained as well.

Langmuir and Brunauer–Emmett–Teller (BET) models were used to fit the adsorption data obtained. All equations and parameters are provided in the ESI.†

Molecular dynamics (MD)

GO-Glu and GO-Met were modelled on a 40 Å × 40 Å graphene sheet created with visual molecular dynamics (MD). The epoxy, hydroxyl, carbonyl, and carboxylic acid groups were randomly positioned on the GO sheet to reproduce the experimental XPS data. Also, the correct grafting density of the amino acids was selected to reproduce the XPS data. The GAFF force field[46] was used to describe GO-Glu and GO-Met. The atomic charges were obtained by AM1 calculations. The GAFF force field was used to parameterize BP4, CBZ and BPA. Atomic charges were obtained by QM calculations at the HF/6-31G(d) level of theory, followed by RESP fitting. All the complexes were inserted into a box of TIP3P water molecules

and counterions were added to neutralise the total charge of the system. MD simulations were carried out using AMBER 16.[47] The systems were minimised using a two-step procedure. In the first step, harmonic constraints (500 kcal mol^{-1} Å^{-2}) were imposed to the molecule/graphene complexes, relaxing only the water molecules and ions. During the second step, all the atoms were free to move. Then, the resulting minimised systems were used as starting points for MD simulations. An equilibration step of 10 ns was carried out by gradually heating the system from 0 to 298 K, using an Andersen thermostat and periodic boundary conditions (PBCs). Then, 100 ns long MD simulations were produced. The molecular mechanics–generalised Born surface area (MM-GBSA) method[49] was applied to compute the binding affinity of BP4, CBZ, and BPA to GO-Glu and GO-Met, extracting the snapshots from the MD trajectories.

## Results and discussion

Synthesis and characterization

The targeted GO-amino acids were synthesised by microwave-assisted epoxide ring opening reaction, as shown in Scheme 1.

The control sample GO-NaOH was also prepared to study possible effects of the experimental conditions of the reaction on the GO structure and their influence on the adsorption properties. The modified GO nanosheets were purified by microfiltration. The cut-off of the microfilter, combined with the purification set-up, allows dynamic washing of the crude within the column, and its separation from the by-products (sketch in Fig. S1, ESI†).

The chemical structure and the amino acid loading ratio for the new modified GO was estimated by X-ray photoelectron spectroscopy (XPS). The survey spectra of amino acid modified GOs are reported in Fig. 1 and their atomic composition is reported in Table 1. The analysed materials were consistent with the typical structure of modified graphene and were mainly composed of carbon, oxygen, and nitrogen, associated with i) the aromatic sp^2 regions of GO, ii) C–O/C=O functional groups, and iii) the nitrogen functional groups (C–N) present in the amino acids. Since C and O are both present in GO and amino acids, the most significant information about the products was obtained from the N 1s signal. The N 1s binding energies of NH$_2$ and NH$_3^+$ were found in the literature:[50] for each amino acid used in this work, the values were contained within the intervals 399.3–399.6 eV and 401.0–401.4 eV. Unfortunately, it was not possible to univocally discriminate between R–NH–R and R–NH$_2$. As a matter of fact, the corresponding binding energies are overlapping, *i.e.* the R–C(O)–NH–R group in polyamic acid at 400.5 eV (ref. 51) or in Nylon 6 at 399.9 eV.[52] The N 1s signal was fitted by two peaks (400.7 eV and 399.4 eV) and one (400.2 eV) peak for GO-Met and GO-Glu, respectively (Fig. S2, ESI†); these binding energies were closer to the R–NH$_2$ or R–NH–R chemical state reported by the literature than to the R–NH$_3^+$ group. The presence of R–NH$_3^+$ was unfavourable because our reaction was performed under basic conditions.

The increase of the N 1s signal (from 0.2% for the reference material GO-NaOH to 0.9% and 0.7% for GO-Glu and GO-Met, respectively) was mainly due to the grafting of the amino acids. It was possible to (roughly) estimate the relative loading of each amino acid from the N 1s peak of GO-Glu and GO-Met. This is possible because most of the N 1s signal arises from the bound amino acid, and because the
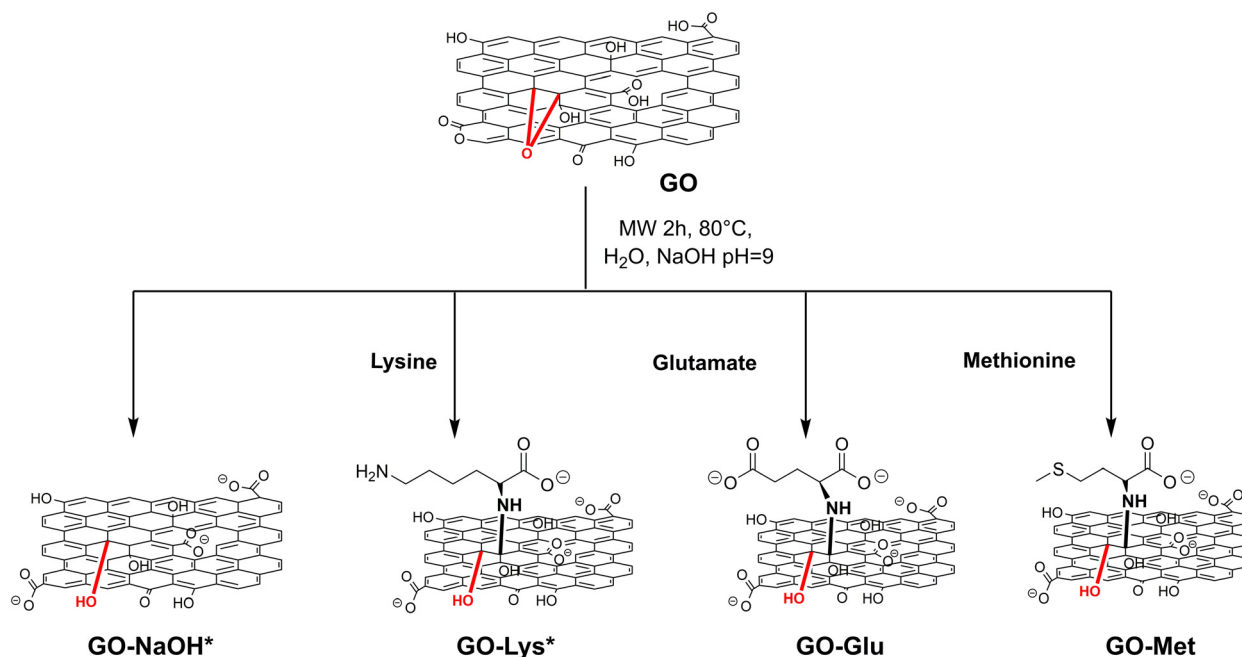
Scheme 1 Synthetic pathway to amino acid–modified GOs. *The detailed syntheses of GO-NaOH and GO-Lys are reported in ref. 43.
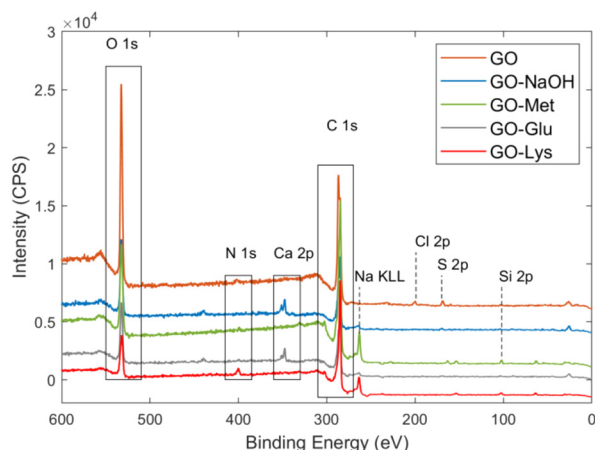
Fig. 1 XPS survey spectra of GO (orange), GO-NaOH (blue), GO-Met (green), GO-Glu (grey), and GO-Lys* (red). *Data from ref. 43.

atomic ratios between N and all other atoms visible by XPS are known from their chemical structure (C, N, O, S). Hydrogen is not detectable by XPS. As further proof of the estimated values, we considered the S (S 2p signal with a S–C chemical shift at 163.4 eV, Fig. S3, ESI†) in GO-Met and estimated the same loading values obtained by N content estimation. It is noteworthy that sulfur was also present in the pristine GO in its typical oxidized form ($R–SO_x$), but the treatment with NaOH removes this group, as confirmed by our experimental evidence (absence of the S 2p signal associated with $R–SO_x$ in GO-Met in Fig. S3† or any other functionalised GO) and some previous dedicated study by Eigler.[53] GO-Glu and GO-Met showed comparable loading, *i.e.* 5% and 6%, respectively. The loading of previously reported GO-Lys was significantly higher being about 15%.[43]

Furthermore, the C 1s peaks of GO-Glu and GO-Met were deconvoluted into their component peaks (see Fig. S4 and Table S1, ESI†). From the deconvolution of the C1s signal of GO-Glu, it is possible to observe the increase in the relative amount of carbon sp^2 (43%) compared to the starting GO (31%) as well as for the reference material GO-NaOH (51%). Similarly, the relative amount of carbon sp^2 for GO-Met (46%) is also increased. XPS revealed the presence of a small percentage of residual Na (reaction in NaOH) and Ca (washing procedure).

Elemental analysis (EA) on pristine amino acid and on modified GOs was performed to analyse the bulk composition. The atomic composition (H, C, O, S) of each material was in good accordance with that estimated by XPS, and is reported in Tables S2–S4, ESI.†

In the free amino acid references, the N/C atomic ratio (and S/C in Met) was exactly the expected one from the molecular structure, while the O/C and H/C ratios were higher, due to the residual water content. After functionalization of GO, the amount of N increases with respect to GO-NaOH, which was taken as a reference instead of GO, since it was subjected to the same reaction conditions and further purification used for amino acid-modified GOs. The observed O/C ratio was systematically overestimated by elemental analysis with respect to XPS, being 0.77 (EA) *vs.* 0.38 (XPS) for GO, 0.92 (EA) *vs.* 0.36 (XPS) for GO-NaOH, 0.49 (EA) *vs.* 0.19 (XPS) for GO-Met, 0.67 (EA) *vs.* 0.26 (XPS) for GO-Glu, and 0.62 (EA) *vs.* 0.14 (XPS) for GO-Lys.

The observed difference can be ascribed to the different environmental conditions during the measurements of EA and XPS. Indeed, XPS is performed in an ultra-high vacuum, with almost no residual water, while EA is carried out under ambient room conditions; and XPS is surface sensitive (a few nm), while EA is bulk sensitive.

The N/C trend (Tables S2 and S3, ESI†), which is not affected by water residuals, was in good accordance with that observed by XPS and confirmed the amino acid loading ratio measured by XPS. Overall, the good accordance between XPS (surface) and EA (bulk) data suggested that the reaction between the amino acids and GO nanosheet surface has occurred.

The O/C ratio of pristine amino acids was similar to or higher than GO, while, after the functionalization, we observed a systematic decrease of the oxidation degree (XPS O%, XPS and EA O/C ratio); thus, the net loss of oxygen after the functionalization has further changed the surface chemistry of GO, which can be summarised as i) the presence of pendant molecules (the amino acid) and ii) the general decrease of C–O/C=O groups. To distinguish the two effects we have taken into consideration reduced GO (rGO), which has a comparable oxidation degree with the amino acid-functionalised GOs (Table 1). The zeta potentials (ζ potentials) of GO and modified GO nanosheets were measured in deionized water. The obtained values, −42.4 ±

Table 1 Atomic composition of amino acid modified graphene materials. Errors on C and O were about ±0.9%, and errors on N, Na, Cl, S and Ca were about ±0.1%. Si was present in quantities <1% in GO-Lys and GO-Met

Material	Atomic composition (%)							Loading%
	C	O	N	Na	Cl	S	Ca	
GO[a]	70.4	27	0.7	—	0.8	1.0	—	
GO-NaOH[a]	70.4	25.6	0.2	0.2	0.3	—	3.3	
GO-Lys[a]	81.5	13.9	3.1	1.2	0.2	—	—	15
GO-Met	81.2	15.6	0.9	0.7	—	0.8	—	5
GO-Glu	77.1	19.7	0.7	0.2	—	—	2.3	6
rGO[b]	86.1	13.7	—	—	0.2	—	—	

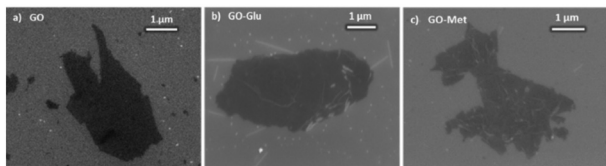[a] Data from ref. 43. [b] Data from ref. 48.

Fig. 2 SEM FEG images of a) GO, b) GO-Glu, and c) GO-Met.

1.2 mV for GO-Glu and −49.6 ± 1.4 mV for GO-Met, were comparable to the ones measured for pristine GO (−43.1 ± 2.4 mV) and GO-Lys (−35.2 ± 0.8 mV), meaning that the surface charge cannot explain the observed different adsorption properties.[43]

The morphology of the modified graphene was investigated by scanning electron microscopy (SEM) showing the typical GO nanosheet morphology for GO-Glu and GO-Met, with a lateral size of a few micrometres, but more aggregated and multilayer nanosheets (Fig. 2).

Adsorption kinetic test

Adsorption selectivity and kinetic studies were carried out on GO, GO-NaOH, GO-Lys, GO-Met, and GO-Glu by measuring the removal of each contaminant from the mixture in the tap water matrix (Fig. 3a), at different contact times (1 h, 4 h, and 24 h). GO and modified GOs were sonicated for 2 h to exfoliate the bulk material into monolayer nanosheets.[54] Different contact times and modified GOs are reported in the ESI† (Fig. S5). Most of the adsorption occurred during the first hours of treatment since no significant differences in removal efficiency were observed between 4 h and 24 h (Fig. S5, ESI†).

Fig. 3b shows the histogram of the adsorption of the different modified GOs, after 4 h of contact time, for each contaminant. Under the selected conditions, GO showed lower

performance for caffeine (CAF), benzophenone-4 (BP4), carbamazepine (CBZ), bisphenol A (BPA), and diclofenac (DCF). The amino acid functionalization changes the surface chemistry of the nanosheets and increases the adsorption selectivity toward the selected contaminants. In fact, modified GOs showed better performance than unmodified GO in the removal of the contaminants that were not completely adsorbed from GO-NaOH (*i.e.* CAF, BP4, CBZ, BPA and DCF).

Adsorption isotherms

Adsorption isotherms were obtained on modified GO for BP4, BPA, and CBZ to investigate the adsorption mechanisms and to estimate the maximum adsorption capacities (more details are reported in ESI,† section 6). The results were compared to those of GO, GO-NaOH, and rGO, and the adsorption isotherms for BPA are reported in Fig. 4, while the isotherms for BP4 and CBZ are reported in the ESI† (Fig. S6, ESI†). Two models were used to fit the isotherms: i) the BET model, which considers multilayer adsorption, where the molecule–molecule interaction is comparable to the molecule–substrate one, and ii) the Langmuir model, which considers a single monolayer and a much stronger molecule–substrate interaction. As previously demonstrated,[43] the adsorption capacity of GO toward the selected molecules was low and it could be described by the BET model as well as by the Langmuir model. As a matter of a fact, the goodness of fit was found to be similar. The treatment with NaOH led to higher adsorption capacity and to a Langmuir model describing the adsorption mechanism. This can be likely ascribed to the different pH values and minor structural modification of GO after NaOH treatment.

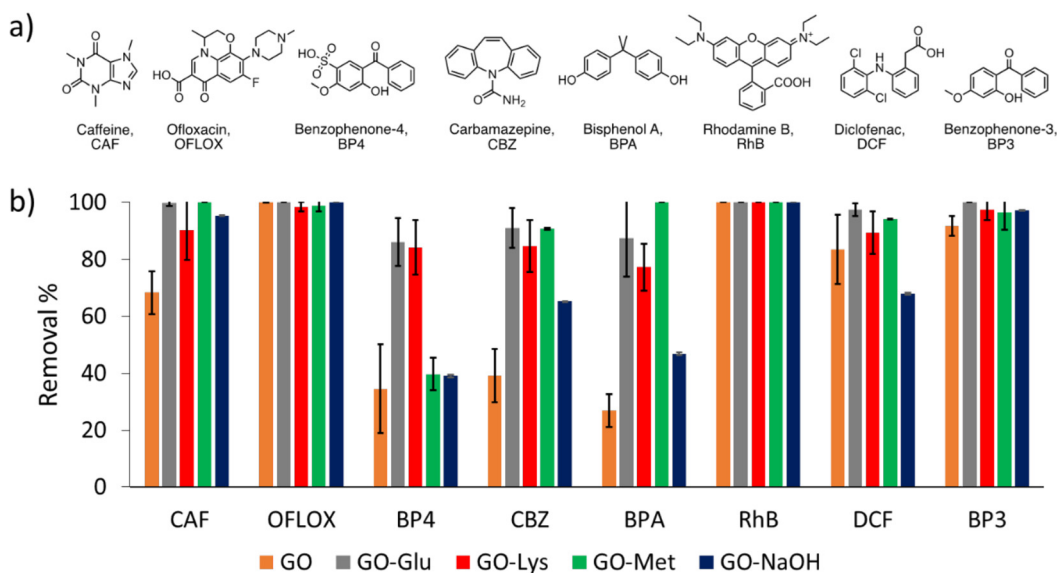A remarkable improvement of adsorption capacity was observed for the amino acid-functionalized GOs. This is not

Fig. 3 a) Molecular structures of selected emerging contaminants. b) Removal of each contaminant from the mixture in tap water (contact time = 4 h, total volume = 10 mL, sorbent amount = 25 mg, C_{IN} = 5 mg L^{-1} of each contaminant) by GO* (orange), GO-Glu (grey), GO-Lys* (red) GO-Met (green) and GO-NaOH* (dark blue). Different contact times are reported in the ESI. *Data from ref. 43.
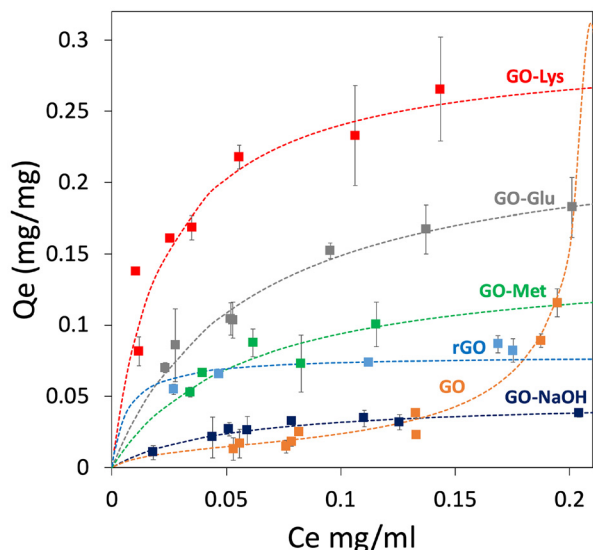
Fig. 4 Adsorption isotherms of BPA. The curves of BP4 and CBZ are reported in the ESI.†

related to a difference in pH, because while the pH of the unmodified GO is acidic (pH = 3.2), each amino acid-modified GO has the same pH of the reference sample GO-NaOH (pH = 8.0). Similarly, the effect of the partial reduction of GO during the reaction with amino acids was studied through the comparison with reduced GO (rGO): with the monolayer adsorption capacity (Qm) of rGO being generally lower than those of amino acid-modified GOs (with exception of BP4 values, Table 2), we can conclude that the reduction contributes to the increase of the number of active adsorption sites, but the main contribution is still from the adsorption sites created by the amino acids.

The Qm values of GO-Met and GO-Glu were significantly higher than those of GO and GO-NaOH, having values always below 80 mg g^{-1} for each contaminant. A different behaviour was observed for the adsorption of BP4. Indeed, the Qm of GO-Glu for BP4 (77 mg g^{-1}) was comparable to that of GO-NaOH (62 mg g^{-1}). In addition, BP4–GO-Glu adsorption was the only one described better by the BET model rather than by the Langmuir model, suggesting that the BP4–BP4 affinity was greater than that of BP4–GO-Glu. Similarly, the

adsorption of CBZ was always better described by the Langmuir model, with comparable Qm values for all modified GO materials (GO-Met 128 mg g^{-1} and GO-Glu 121 mg g^{-1}), including GO-Lys (172 mg g^{-1}).

As shown by Fig. 5, for CBZ the Qm increased almost linearly with the % loading of amino acids (Fig. 5), suggesting that the number of active sites for CBZ adsorption increases as a function of the number of amino acid molecules on the surface, with marginal influence of the amino acid structure. On the other hand, BP4 (and partially BPA) has a step-like increase of the Qm *vs.* loading, which suggests that the active sites for adsorption mainly depend on the chemical environment created by the specific amino acid. Despite being limited to three case studies (*i.e.* three loading amounts), these results clearly show that the amino acid structure may influence the adsorption extent. However, the contaminant molecular structure also plays a key role in the overall adsorption.

Molecular dynamics simulations

Molecular dynamics (MD) simulations were carried out to investigate the interactions between BP4, CBZ, and BPA molecules and the amino acid-modified GOs at an atomistic level, and to explain their adsorption performances with respect to unmodified GO. Indeed, the MD analysis of the contaminant–nanosheet interaction[55] allows the favourite adsorption sites on GO sheets to be identified, thus ultimately providing general rules to identify the thermodynamic forces[56] driving the binding of the contaminants (Table 3 and Fig. 6).

Calculations showed that the molecules of contaminants interact preferentially with the amino acid side chains, grafted on the basal plane of GO (see Fig. 6).

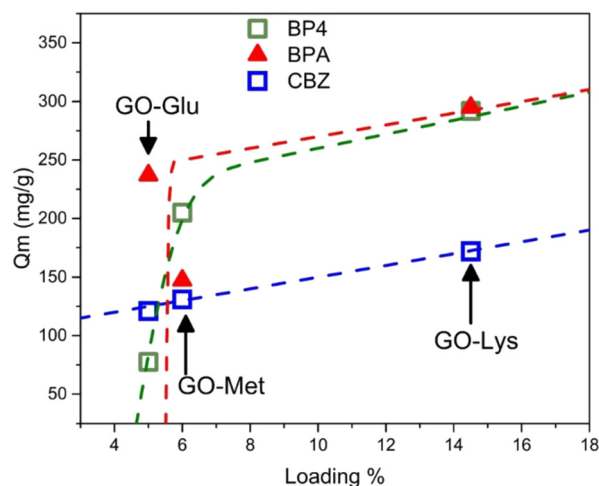This binding mode increases the binding affinity between BP4, CBZ, and BPA and amino acid-modified GOs, when

Table 2 Maximum adsorption capacity (mg g^{-1}) of synthesised materials toward selected contaminants. Best fitting model Langmuir model (L) and BET (B) model marked in the cells

Material	Qm (mg g^{-1})					
	BP4		BPA		CBZ	
GO^a	11 ± 5	(B)	14 ± 5	(B)	7 ± 2	(L)
rGO	115 ± 18	(L)	78 ± 11	(L)	43 ± 13	(L)
GO-NaOH^a	62 ± 12	(L)	48 ± 15	(L)	80 ± 15	(L)
GO-Lys^a	292 ± 30	(L)	295 ± 50	(L)	172 ± 20	(L)
GO-Met	205 ± 20	(L)	147 ± 30	(L)	128 ± 15	(L)
GO-Glu	77.5 ± 20	(B)	237 ± 40	(L)	121 ± 20	(L)

^{a} Data from ref. 43.

Fig. 5 Plot of the maximum adsorption capacity (Qm) calculated through isotherms[43] as a function of the amino acid loading (calculated on N/C).

Table 3 Computed total binding affinity (E_{TOT}) and its contributions *i.e.*, van der Waals (vdW), electrostatic (E_{El}) and non-polar solvation ($E_{non-polar\ solvation}$) for BP4, CBZ and BPA towards GO, GO-Glu and GO-Met. All energies are reported in kcal mol^{-1}

Contaminant	Material	E_{TOT}	E_{El}	$E_{non-polar\ solvation}$
BP4	GO[a]	−11.9	10.1	−1.1
	GO-Glu	−21.1	12.2	−2.8
	GO-Met	−22.0	12.1	−2.9
CBZ	GO[a]	−18.4	4.1	−0.7
	GO-Glu	−20.8	3.6	−2.4
	GO-Met	−21.5	3.9	−2.5
BPA	GO[a]	−15.7	4.4	−0.8
	GO-Glu	−17.1	4.5	−2.0
	GO-Met	−18.9	5.7	−2.5

[a] Values from ref. 43.

compared to GO, in agreement with the experimental results. The energy values involved in the adsorption are reported in Table 3. The total energy of interaction is the sum of three contributions, *i.e.* electrostatic and van der Waals interactions and surface energy (E_{surf}). The electrostatic terms are little sensitive to the adsorption process, since the process happens in water (and simulations are carried out in explicit water molecules), which strongly quenches the coulombic terms due to its high dielectric constant. Consequently, the adsorption extent on oppositely charged (Glu and Lys) or neutral (Met) amino acids was similar. The higher removal observed for the amino-acid modified GOs can be ascribed to the enhanced van der Waals contacts between the surface of the chemically modified nanosheets and BP4, CBZ, and BPA, and to the highest stabilizing $E_{non-polar\ solvation}$ term. This term takes into account the non-polar solvation energy, which is more stabilizing in the case of the modified GOs, as a result of the interaction of the hydrophobic core of the contaminants with the hydrophobic portion of the amino acid side chains, *i.e.* their aliphatic chain. In GO, the stabilizing $E_{non-polar\ solvation}$ term is small and thus the adsorption of the contaminants on the surface of unmodified GO is less favorable than that on the surface of the amino acid-modified GOs.

The adsorption process between carbon nanomaterials and molecules is mainly driven by shape complementarity.[57–59]

Hydrophobic interactions, which govern the binding between the contaminant and the adsorption site, are directly proportional to the van der Waals interactions and $E_{non-polar\ solvation}$. Both these terms depend directly on the contact area between the adsorption site and the contaminant, *i.e.* their shape complementarity (see Fig. 6). As a hydrophobic contaminant occupies one adsorption site, i) new van der Waals interactions are established, ii) cavitation energy is reduced, and iii) associated water molecules are shed (hydrophobic effect). Shape complementarity can be quantitatively measured by calculating the variation of the solvent accessible surface area (ΔSASA, Fig. 6) upon binding.

Consequently, the observed improvement in adsorption capacity can be ascribed to the increased shape complementarity between BP4, CBZ, and BPA and the amino acid modified GO nanosheets (Fig. S10 and Table S11†) through 3D recognition sites formed on the nanosheet surface after chemical modification. This effect is more evident with non-planar/bent molecules, such as BP4, CBZ, and BPA, which benefit most from the formation of a "local corrugation" on the 2D basal plane of GO.
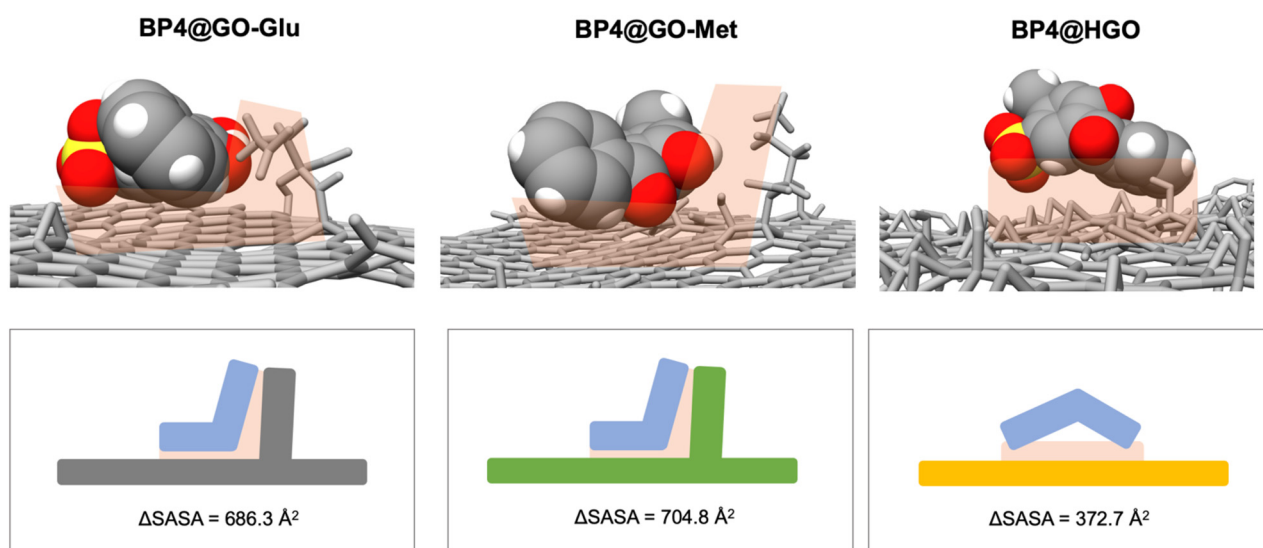

Fig. 6 Contact area in the interaction between BP4 and GO-Glu (left column), GO-Met (middle column) and GO (right column) sheets. ΔSASA measurement quantifies the contact area between the contaminant and the different sorbents (shape complementarity) and it is proportional to their binding energies and removal efficiency. Results on GO-Lys are reported in ref. 43.

Conclusions

Graphene oxide (GO) was functionalized with L-glutamic acid and L-methionine by a fast and efficient microwave-assisted protocol, and worked up with a standardized purification protocol based on microfiltration on commercial modules. The synthetic approach allowed high purity of the reaction products, with a high batch to batch reproducibility, thanks to the standard microfiltration module features. Structure analysis revealed amino acid loadings in the range of 5–15%, with partial reduction of GO (from 27% down to 14–20% of oxygen). Adsorption of a mixture of eight contaminants in tap water was studied for amino acid-modified GOs and compared to unmodified GO and rGO. As a further control sample, we considered also GO subjected to the reaction conditions but treated in the absence of any amino acid, called GO-NaOH. This systematic study allowed us to unambiguously unravel the role of the amino acid binding in the adsorption properties of GO. The removal of most of the targeted contaminants occurred in the first hour of treatment, with a significant improvement of the removal of BPA, CBZ, and BP4 observed for the modified materials. Adsorption isotherms show that the Langmuir model describes the adsorption mechanism better than the BET model, except for the pairs BP4–GO-Glu, BP4–GO, and BPA–GO. In addition, the maximum adsorption capacities (Qm) for the amino acid-modified GOs were found to be in the range of 77–292 mg g^{-1} for BP4, 147–295 mg g^{-1} for BPA, and 121–172 mg g^{-1} for CBZ, with GO-Lys expressing the best performance in each case. Qm was found to be strictly dependent on the amino acid loading, which suggests an active role in the removal of contaminant molecules by the grafting procedure. Accordingly, molecular dynamics simulations revealed higher interaction energies for amino acid-modified GOs rather than unmodified GO, which may be ascribed to the higher van der Waals and hydrophobic interactions between the amino acid hydrophobic chain and the contaminant molecules. The grafting of amino acids forms 3D recognition sites on the surface of the GO nanosheets, which improve the removal capacity of the modified materials.

In conclusion, our results will promote the design of new graphenic sorbents for water treatment, with tuneable and predictable adsorption capacity on selected contaminants. Future work on these new sorbents will be dedicated to their exploitation for the purification of different water matrices and to the development of microfiltration based regeneration of the exhausted nanomaterials.

Author contributions

The authors contributed equally to this work.

Conflicts of interest

There are no conflicts to declare.

Acknowledgements

Notes and references

1 *EEA Report No 09/2021*, **https://www.eea.europa.eu/ publications/drivers-of-and-pressures-arising.**

2 S. Sharma and A. Bhattacharya, Drinking water contamination and treatment techniques, *Appl. Water Sci.*, 2017, **7**(3), 1043–1067.

3 S. González-Rubio, A. Ballesteros-Gómez, A. G. Asimakopoulos and V. L. B. Jaspers, A review on contaminants of emerging concern in European raptors (2002–2020), *Sci. Total Environ.*, 2021, **760**, 143337.

4 J. Fick, H. Söderström, R. H. Lindberg, C. Phan, M. Tysklind and D. G. J. Larsson, Contamination of surface, ground, and drinking water from pharmaceutical production, *Environ. Toxicol. Chem.*, 2009, **28**(12), 2522–2527.

5 *ECHA*, E. C. A. Candidate List ofsubstances of very high concern for authorisation, **https://echa.europa.eu/it/ candidate-list-table**.

6 S. Sorlini, M. Collivignarelli and M. Carnevale Miino, Technologies for the control of emerging contaminats in drinking water treatment plants, *Environ. Eng. Manage. J.*, 2019, **18**, 2203–2216.

7 R. Kumar, M. Qureshi, D. K. Vishwakarma, N. Al-Ansari, A. Kuriqi, A. Elbeltagi and A. Saraswat, A review on emerging water contaminants and the application of sustainable removal technologies, *Case Stud. Chem. Environ. Eng.*, 2022, **6**, 100219.

8 N. Caporale, M. Leemans, L. Birgersson, P.-L. Germain, C. Cheroni, G. Borbély, E. Engdahl, C. Lindh, R. B. Bressan, F. Cavallo, N. E. Chorev, G. A. D'Agostino, S. M. Pollard, M. T. Rigoli, E. Tenderini, A. L. Tobon, S. Trattaro, F. Troglio, M. Zanella, Å. Bergman, P. Damdimopoulou, M. Jönsson, W. Kiess, E. Kitraki, H. Kiviranta, E. Nånberg, M. Öberg, P. Rantakokko, C. Rudén, O. Söder, C.-G. Bornehag, B. Demeneix, J.-B. Fini, C. Gennings, J. Rüegg, J. Sturve and G. Testa, From cohorts to molecules: Adverse impacts of endocrine disrupting mixtures, *Science*, 2022, **375**(6582), eabe8244.

9 V. Kayastha, J. Patel, N. Kathrani, S. Varjani, M. Bilal, P. L. Show, S.-H. Kim, E. Bontempi, S. K. Bhatia and X.-T. Bui, New Insights in factors affecting ground water quality with focus on health risk assessment and remediation techniques, *Environ. Res.*, 2022, **212**, 113171.

10 C. G. Bornehag, C. Lindh, A. Reichenberg, S. Wikström, M. Unenge Hallerback, S. F. Evans, S. Sathyanarayana, E. S. Barrett, R. H. N. Nguyen, N. R. Bush and S. H. Swan, Association of Prenatal Phthalate Exposure With Language Development in Early Childhood, *JAMA Pediatr.*, 2018, **172**(12), 1169–1176.

11 Y. Ben, C. Fu, M. Hu, L. Liu, M. H. Wong and C. Zheng, Human health risk assessment of antibiotic resistance

associated with antibiotic residues in the environment: A review, *Environ. Res.*, 2019, **169**, 483–493.

12 N. Cheng, B. Wang, P. Wu, X. Lee, Y. Xing, M. Chen and B. Gao, Adsorption of emerging contaminants from water and wastewater by modified biochar: A review, *Environ. Pollut.*, 2021, **273**, 116448.

13 N. A. Ahammad, M. A. Ahmad, B. H. Hameed and A. T. Mohd Din, A mini review of recent progress in the removal of emerging contaminants from pharmaceutical waste using various adsorbents, *Environ. Sci. Pollut. Res.*, 2022, DOI: 10.1007/s11356-022-19829-0.

14 M. Varsha, P. Senthil Kumar and B. Senthil Rathi, A review on recent trends in the removal of emerging contaminants from aquatic environment using low-cost adsorbents, *Chemosphere*, 2022, **287**, 132270.

15 F. Perreault, A. Fonseca de Faria and M. Elimelech, Environmental applications of graphene-based nanomaterials, *Chem. Soc. Rev.*, 2015, **44**(16), 5861–5896.

16 P. L. Yap, M. J. Nine, K. Hassan, T. T. Tung, D. N. H. Tran and D. Losic, Graphene-Based Sorbents for Multipollutants Removal in Water: A Review of Recent Progress, *Adv. Funct. Mater.*, 2021, **31**(9), 2007356.

17 S. Khaliha, T. D. Marforio, A. Kovtun, S. Mantovani, A. Bianchi, M. L. Navacchia, M. Zambianchi, L. Bocchi, N. Boulanger, A. Iakunkov, M. Calvaresi, A. V. Talyzin, V. Palermo and M. Melucci, Defective graphene nanosheets for drinking water purification: Adsorption mechanism, performance, and recovery, *FlatChem*, 2021, **29**, 100283.

18 S. Khaliha, A. Bianchi, A. Kovtun, F. Tunioli, A. Boschi, M. Zambianchi, D. Paci, L. Bocchi, S. Valsecchi, S. Polesello, A. Liscio, M. Bergamini, M. Brunetti, M. L. Navacchia, V. Palermo and M. Melucci, Graphene oxide nanosheets for drinking water purification by tandem adsorption and microfiltration, *Sep. Purif. Technol.*, 2022, **300**, 121826.

19 S. Mantovani, S. Khaliha, L. Favaretto, C. Bettini, A. Bianchi, A. Kovtun, M. Zambianchi, M. Gazzano, B. Casentini, V. Palermo and M. Melucci, Scalable synthesis and purification of functionalized graphene nanosheets for water remediation, *Chem. Commun.*, 2021, **57**(31), 3765–3768.

20 M. Zambianchi, M. Durso, A. Liscio, E. Treossi, C. Bettini, M. L. Capobianco, A. Aluigi, A. Kovtun, G. Ruani, F. Corticelli, M. Brucale, V. Palermo, M. L. Navacchia and M. Melucci, Graphene oxide doped polysulfone membrane adsorbers for the removal of organic contaminants from water, *Chem. Eng. J.*, 2017, **326**, 130–140.

21 M. Zambianchi, S. Khaliha, A. Bianchi, F. Tunioli, A. Kovtun, M. L. Navacchia, A. Salatino, Z. Xia, E. Briñas, E. Vázquez, D. Paci, V. Palermo, L. Bocchi, B. Casentini and M. Melucci, Graphene oxide-polysulfone hollow fibers membranes with synergic ultrafiltration and adsorption for enhanced drinking water treatment, *J. Membr. Sci.*, 2022, **658**, 120707.

22 A. Kovtun, A. Bianchi, M. Zambianchi, C. Bettini, F. Corticelli, G. Ruani, L. Bocchi, F. Stante, M. Gazzano, T. D. Marforio, M. Calvaresi, M. Minelli, M. L. Navacchia, V. Palermo and M. Melucci, Core–shell graphene oxide–polymer hollow fibers as water filters with enhanced

performance and selectivity, *Faraday Discuss.*, 2021, **227**(0), 274–290.

23 L. Y. Ng, H. S. Chua and C. Y. Ng, Incorporation of graphene oxide-based nanocomposite in the polymeric membrane for water and wastewater treatment: A review on recent development, *J. Environ. Chem. Eng.*, 2021, **9**(5), 105994.

24 X. Wang, Y. Zhao, E. Tian, J. Li and Y. Ren, Graphene Oxide-Based Polymeric Membranes for Water Treatment, *Adv. Mater. Interfaces*, 2018, **5**(15), 1701427.

25 A. Kovtun, M. Zambianchi, C. Bettini, A. Liscio, M. Gazzano, F. Corticelli, E. Treossi, M. L. Navacchia, V. Palermo and M. Melucci, Graphene oxide–polysulfone filters for tap water purification, obtained by fast microwave oven treatment, *Nanoscale*, 2019, **11**(47), 22780–22787.

26 A. Nordenström, N. Boulanger, A. Iakunkov, I. Baburin, A. Klechikov, A. Vorobiev and A. V. Talyzin, Intercalation of Dyes in Graphene Oxide Thin Films and Membranes, *J. Phys. Chem. C*, 2021, **125**(12), 6877–6885.

27 N. Boulanger, A. S. Kuzenkova, A. Iakunkov, A. Y. Romanchuk, A. L. Trigub, A. V. Egorov, S. Bauters, L. Amidani, M. Retegan, K. O. Kvashnina, S. N. Kalmykov and A. V. Talyzin, Enhanced Sorption of Radionuclides by Defect-Rich Graphene Oxide, *ACS Appl. Mater. Interfaces*, 2020, **12**(40), 45122–45135.

28 A. Nordenström, N. Boulanger, A. Iakunkov, G. Li, R. Mysyk, G. Bracciale, P. Bondavalli and A. V. Talyzin, High-surface-area activated carbon from pine cones for semi-industrial spray deposition of supercapacitor electrodes, *Nanoscale Adv.*, 2022, 4689–4700.

29 P. L. Yap, S. Kabiri, Y. L. Auyoong, D. N. H. Tran and D. Losic, Tuning the Multifunctional Surface Chemistry of Reduced Graphene Oxide via Combined Elemental Doping and Chemical Modifications, *ACS Omega*, 2019, **4**(22), 19787–19798.

30 Y. Shen, Q. Fang and B. Chen, Environmental Applications of Three-Dimensional Graphene-Based Macrostructures: Adsorption, Transformation, and Detection, *Environ. Sci. Technol.*, 2015, **49**(1), 67–84.

31 D. Tian, D. Geng, W. Tyler Mehler, G. Goss, T. Wang, S. Yang, Y. Niu, Y. Zheng and Y. Zhang, Removal of perfluorooctanoic acid (PFOA) from aqueous solution by amino-functionalized graphene oxide (AGO) aerogels: Influencing factors, kinetics, isotherms, and thermodynamic studies, *Sci. Total Environ.*, 2021, **783**, 147041.

32 V. W. O. Wanjeri, C. J. Sheppard, A. R. E. Prinsloo, J. C. Ngila and P. G. Ndungu, Isotherm and kinetic investigations on the adsorption of organophosphorus pesticides on graphene oxide based silica coated magnetic nanoparticles functionalized with 2-phenylethylamine, *J. Environ. Chem. Eng.*, 2018, **6**(1), 1333–1346.

33 K. Spyrou, M. Calvaresi, E. K. Diamanti, T. Tsoufis, D. Gournis, P. Rudolf and F. Zerbetto, Graphite Oxide and Aromatic Amines: Size Matters, *Adv. Funct. Mater.*, 2015, **25**(2), 263–269.

34 M. Yan, Q. Liang, W. Wan, Q. Han, S. Tan and M. Ding, Amino acid-modified graphene oxide magnetic nanocomposite for the magnetic separation of proteins, *RSC Adv.*, 2017, **7**(48), 30109–30117.

35 A. O. E. Abdelhalim, V. V. Sharoyko, A. A. Meshcheriakov, M. D. Luttsev, A. A. Potanin, N. R. Iamalova, E. E. Zakharov, S. V. Ageev, A. V. Petrov, L. V. Vasina, I. L. Solovtsova, A. V. Nashchekin, I. V. Murin and K. N. Semenov, Synthesis, characterisation and biocompatibility of graphene–L-methionine nanomaterial, *J. Mol. Liq.*, 2020, **314**, 113605.

36 I. A. Vacchi, C. Spinato, J. Raya, A. Bianco and C. Ménard-Moyon, Chemical reactivity of graphene oxide towards amines elucidated by solid-state NMR, *Nanoscale*, 2016, **8**(28), 13714–13721.

37 C. Jiang, X. Wang, B. Hou, C. Hao, X. Li and J. Wu, Construction of a Lignosulfonate–Lysine Hydrogel for the Adsorption of Heavy Metal Ions, *J. Agric. Food Chem.*, 2020, **68**(10), 3050–3060.

38 H. Ge and W. Zou, Preparation and characterization of L-glutamic acid-functionalized graphene oxide for adsorption of Pb(II), *J. Dispersion Sci. Technol.*, 2017, **38**(2), 241–247.

39 W. Li, Q. Liu, J. Liu, H. Zhang, R. Li, Z. Li, X. Jing and J. Wang, Removal U(VI) from artificial seawater using facilely and covalently grafted polyacrylonitrile fibers with lysine, *Appl. Surf. Sci.*, 2017, **403**, 378–388.

40 J. Xiao, W. Lv, Z. Xie, Y. Song and Q. Zheng, l-cysteine-reduced graphene oxide/poly(vinyl alcohol) ultralight aerogel as a broad-spectrum adsorbent for anionic and cationic dyes, *J. Mater. Sci.*, 2017, **52**, 13626–13635.

41 Y.-R. Zhang, P. Su, J. Huang, Q.-R. Wang and B.-X. Zhao, A magnetic nanomaterial modified with poly-lysine for efficient removal of anionic dyes from water, *Chem. Eng. J.*, 2015, **262**, 313–318.

42 S. Yadav, A. Asthana, A. K. Singh, R. Chakraborty, S. S. Vidya, A. Singh and S. A. C. Carabineiro, Methionine-Functionalized Graphene Oxide/Sodium Alginate Bio-Polymer Nanocomposite Hydrogel Beads: Synthesis, Isotherm and Kinetic Studies for an Adsorptive Removal of Fluoroquinolone Antibiotics, *Nanomaterials*, 2021, **11**(3), 568.

43 S. Mantovani, S. Khaliha, T. D. Marforio, A. Kovtun, L. Favaretto, F. Tunioli, A. Bianchi, G. Petrone, A. Liscio, V. Palermo, M. Calvaresi, M. L. Navacchia and M. Melucci, Facile high-yield synthesis and purification of lysine-modified graphene oxide for enhanced drinking water purification, *Chem. Commun.*, 2022, **58**(70), 9766–9769.

44 https://www.medica.it/.

45 A. Pintus, S. Mantovani, A. Kovtun, G. Bertuzzi, M. Bandini and M. Melucci, Recyclable GO-Arginine Hybrids for CO2 Fixation into Cyclic Carbonates, *Chem. – Eur. J.*, 2022, DOI: 10.1002/chem.202202440.

46 J. Wang, R. M. Wolf, J. W. Caldwell, P. A. Kollman and D. A. Case, Development and testing of a general amber force field, *J. Comput. Chem.*, 2004, **25**(9), 1157–1174.

47 D. A. Case, R. MB, D. S. Cerutti, T. E. Cheatham III, T. A. Darden, R. E. Duke, T. J. Giese, H. Gohlke, A. W. Goetz, N. Homeyer, S. Izadi, P. Janowski, J. Kaus, A. Kovalenko, T. S. Lee, S. LeGrand, P. Li, C. Lin, T. Luchko, R. Luo, B. Madej, D. Mermelstein, K. M. Merz, G. Monard, H. Nguyen, H. T. Nguyen, I. Omelyan, A. Onufriev, D. R. Roe, A. Roitberg, C.

Sagui, C. L. Simmerling, W. M. Botello-Smith, J. Swails, R. C. Walker, J. Wang, R. M. Wolf, X. Wu, L. Xiao and P. A. Kollman, *AMBER*, University of California, San Francisco, 2016.

48 L. Lombardi, A. Kovtun, S. Mantovani, G. Bertuzzi, L. Favaretto, C. Bettini, V. Palermo, M. Melucci and M. Bandini, Visible-Light Assisted Covalent Surface Functionalization of Reduced Graphene Oxide Nanosheets with Arylazo Sulfones, *Chem. – Eur. J.*, 2022, **28**(26), e202200333.

49 B. R. Miller III, T. D. McGee Jr., J. M. Swails, N. Homeyer, H. Gohlke and A. E. Roitberg, MMPBSA.py: An Efficient Program for End-State Free Energy Calculations, *J. Chem. Theory Comput.*, 2012, **8**(9), 3314–3321.

50 A. Artemenko, A. Shchukarev, P. Štenclová, T. Wågberg, J. Segervald, X. Jia and A. Kromka, Reference XPS spectra of amino acids, *IOP Conf. Ser.: Mater. Sci. Eng.*, 2021, **1050**(1), 012001.

51 J. Russat, Characterization of polyamic acid/polyimide films in the nanometric thickness range from spin-deposited polyamic acid, *Surf. Interface Anal.*, 1988, **11**(8), 414–420.

52 P. Louette, F. Bodino and J.-J. Pireaux, Nylon 6 (N6) Reference XPS Reference Core Level and Energy Loss Spectra, *Surf. Sci. Spectra*, 2005, **12**(1), 12–17.

53 T. J. Nacken, C. E. Halbig, S. E. Wawra, C. Damm, S. Romeis, J. Walter, M. J. Tehrani, Y. Hu, Y. Ishii, S. Eigler and W. Peukert, Structural factors controlling size reduction of graphene oxide in liquid processing, *Carbon*, 2017, **125**, 360–369.

54 A. Liscio, K. Kouroupis-Agalou, X. D. Betriu, A. Kovtun, E. Treossi, N. M. Pugno, G. De Luca, L. Giorgini and V. Palermo, Evolution of the size and shape of 2D nanosheets during ultrasonic fragmentation, *2D Mater.*, 2017, **4**(2), 025017.

55 M. Calvaresi and F. Zerbetto, Atomistic molecular dynamics simulations reveal insights into adsorption, packing, and fluxes of molecules with carbon nanotubes, *J. Mater. Chem. A*, 2014, **2**(31), 12123–12135.

56 M. Calvaresi, A. Bottoni and F. Zerbetto, Thermodynamics of Binding Between Proteins and Carbon Nanoparticles: The Case of C60@Lysozyme, *J. Phys. Chem. C*, 2015, **119**(50), 28077–28082.

57 M. Di Giosia, T. D. Marforio, A. Cantelli, F. Valle, F. Zerbetto, Q. Su, H. Wang and M. Calvaresi, Inhibition of α-chymotrypsin by pristine single-wall carbon nanotubes: Clogging up the active site, *J. Colloid Interface Sci.*, 2020, **571**, 174–184.

58 M. Di Giosia, F. Valle, A. Cantelli, A. Bottoni, F. Zerbetto, E. Fasoli and M. Calvaresi, Identification and preparation of stable water dispersions of protein - Carbon nanotube hybrids and efficient design of new functional materials, *Carbon*, 2019, **147**, 70–82.

59 M. Di Giosia, F. Zerbetto and M. Calvaresi, Incorporation of Molecular Nanoparticles Inside Proteins: The Trojan Horse Approach in Theranostics, *Acc. Mater. Res.*, 2021, **2**(8), 594–605.